THEORETICAL
INORGANIC CHEMISTRY

Optical Band Gap Energies in Quasi-Metal Carbon Nanotubes

P. N. D'yachkov

Kurnakov Institute of General and Inorganic Chemistry, Russian Academy of Sciences Moscow, 119991 Russia
e-mail: p_dyachkov@rambler.ru
Received February 27, 2017

Abstract—The structure of carbon nanotubes is described by two positive integers (n_1,n_2). The π-electron model of the nanotube band structure predicts that when the difference $n_1 - n_2$ is multiple of three, the energy gap between the valence and conduction bands vanishes so that such tubes should exhibit quasi-metal properties. The band structure of 50 chiral and achiral (n_1,n_2) nanotubes with $4 \leq n_1 \leq 18$ and $n_2 = n_1 - 3q$ has been calculated by the linearized augmented cylindrical wave method. Nanotubes have been identified for which the optical band gaps are in the terahertz range (1−40 meV) and which can be used for design of emitters, detectors, multipliers, antennas, transistors, and other nanoelements operating in the high-frequency range.

Carbon nanotubes are giant molecules that have cylindrical surfaces tiled with benzene hexagons. There is a strong relationship between the geometry and band structure of graphene (graphite sheet) and nanotubes. The structure of any nanotube can be obtained by rolling the graphene sheet into a cylinder. The nanotube geometry can be described by two positive integers (n_1,n_2), which specify the nanotube diameter and orientation of benzene hexagons with respect to the cylinder axis. Neglecting the surface curvature of a nanotube makes it possible to determine the π-electron band structure of nanotubes as a result of projecting the π-bands of graphene onto the cylinder surface [1−5]. This approximation demonstrates that nanotubes with $n_1 = n_2$ has metal conductance due to the overlap of the π-bands at the Fermi level. The (n_1,n_2) nanotubes with the $n_1 - n_2$ differences other than a multiple of three should be semiconductors with a band gap from a few tenths of an electron volt to 1 eV. If the $n_1 - n_2$ difference is a multiple of three, the top of the valence band and the bottom of the conduction band touch each other and, hence, there is no optical band gap in the nanotube, so that it should have semimetallic properties. However, in the latter case, taking into account the nanotube surface curvature sharply changes the prediction and demonstrates that nanotubes should be actually narrow-gap semiconductors with optical band gaps that can fall into the terahertz (THz) range 0.1−40 meV [6−17], which enables their use as terahertz emitters, detectors, polarizers, and multipliers, as well as pn-junctions and transistors with properties that can be tailored by applying weak external electromagnetic field [18−30].

It has been noted that the minigap energies in quasi-metallic nanotubes are determined not only by purely band factors [20, 21, 31]. For example, the band gap energies measured for the nanotubes located on a substrate and in the free state can differ up to ten times due to the charge carrier trapping in the substrate [32]. It is not quite clear whether one-electron or collective electronic excitations determine the experimentally observed band gaps [20, 21, 31]. Finally, synthesis of nanotubes can generate mechanical strains, which can also lead to the formation of band gaps near the Fermi level.

Standard quantum-chemical calculations using basis sets of plane waves or atomic orbitals with inclusion of translational symmetry of nanotubes turned out to be inefficient for determining band gap energies in chiral narrow-gap nanotubes with giant unit cells; only a small number of such calculations dealing only with zigzag $(n,0)$ nanotubes is available. The aim of the present study is to fill this gap, namely, to determine the band structures of achiral and chiral nanotubes with $n_1 - n_2 = 3q$, where $q = 1, 2...$, by the linearized augmented cylindrical wave (LACW) method.

COMPUTATIONAL DETAILS

The LACW method is an extension of Slater's augmented plane wave method, well-known in the band theory of crystals [33−36], to the case of cylindrical polyatomic systems. Both methods use the local-density approximation for the electron potential, and the potential is taken to be spherically symmetric in the vicinity of atoms and constant in the interatomic space. Computational specific features of the method and its application have been described elsewhere [37−42].
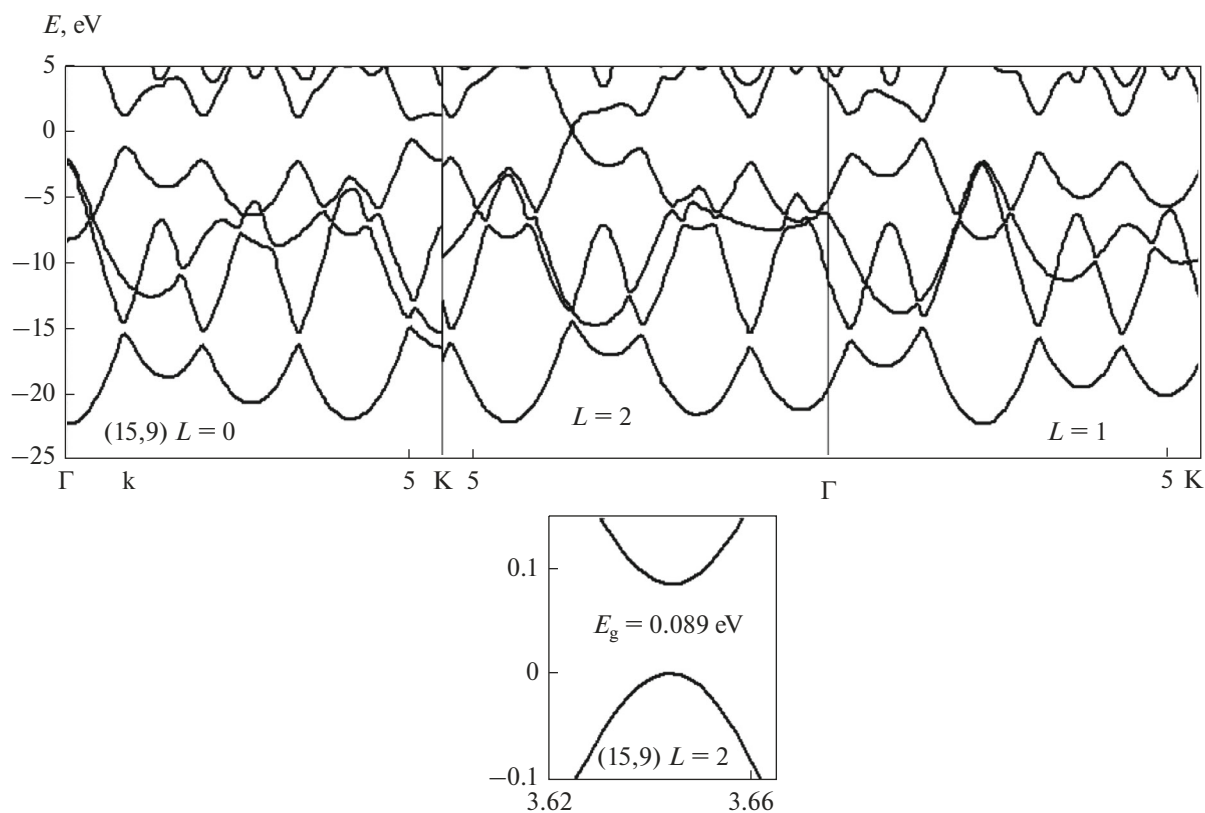
Fig. 1. An example of the band structure calculated by the LACW method. Here, the full band structure of the (15,9) tube is shown, and the band gap region is displayed on an enlarged scale.

In ab initio calculations of nanotubes, all their symmetry properties should be considered. The (n_1,n_2) nanotubes have rotational symmetry axis C_n, where n is the greatest common divisor of n_1 and n_2. In addition, the tube structure is invariant under the action of screw translations $S(h, \omega)$—translations h along the nanotube axis with rotations ω about this axis, which are calculated by the formulas

$$h = \frac{3d_{C-C}}{2} \frac{n}{\left(n_1^2 + n_2^2 + n_1 n_2\right)^{1/2}}, \quad (1)$$

$$\omega = 2\pi \frac{n_1 p_1 + n_2 p_2 + (n_1 p_2 + n_2 p_1)/2}{n_1^2 + n_2^2 + n_1 n_2}. \quad (2)$$

Here, $d_{C-C} = 1.42$ Å is the C–C bond length, and positive integers p_1 and p_2 are found from the equation $p_2 n_1 - p_1 n_2 = n$.

If the rotational and screw symmetry of a nanotube is considered, its unit cell is reduced to two atoms, and the LACW method is applicable to calculations of all nanotubes irrespective of their diameter and chirality [39]. The band structure of tubes is described by four valence band curves and low-energy conduction band curves depending on the wave vector $0 \le k \le \pi/h$ and rotational quantum number $L = 0, 1, ..., n - 1$, as shown

in Fig. 1, which presents, as an example, the full band structure of the (15,9) nanotube and its band gap.

COMPUTATION DETAILS

The computation results are summarized in Table 1, which gives the band gap width in the nanotubes and their structural characteristics—screw axis parameters h and ω, radii R, and chirality angles of nanotubes.

Let us begin with discussing eight nanotubes with $4 \le n_1 \le 8$ and small radii R. Because of the large surface curvature of these tubes, the Hückel π-electron model is not completely applicable here [42]. In particular, nanotubes with $n_1 = 4$, 5, and 6 as well as the (7,1) nanotubes turn out to be metallic, rather then semiconducting, because of the overlap of different dispersion curves at the Fermi level. The (7,4), (8,2), and (8,5) nanotubes of larger radius and smaller curvature have the expected band gaps with energies of 0.125, 0.32, and 0.058 eV, but they are too large for using the these tubes in THz technologies.

In the series of $(9,n_2)$ nanotubes ($n_2 = 0$, 3, and 6), the increase in index n_2 is accompanied by a decrease in the band gap width E_g from 0.19 to 0.11 and 0.035 eV. Such a decrease in the band gap width is consistent with the simple π-electron model in which the

Table 1. Structural parameters and band gap energies of nanotubes with $n_1 - n_2 = 3q$

Nanotube	Structural parameters of a nanotube				Band gap width, eV		
	h, au	ω, rad	R, Å	θ, deg	LACW	exp.	ab initio LCAO
(4,1)	0.878	1.35	1.79	10.5	0		0 [45]
(5,2)	0.643	2.65	2.44	16.1	0		0 [45]
(6,0)	4.02	0	3.35	0	0		0 [45]
(6,3)	1.52	1.34	3.11	19.1	0		0.056 [45]
(7,1)	0.532	0.826	2.96	6.59	0		0.138 [45]
(7,4)	0.417	1.72	3.77	21.1	0.125		0.067 [45]
(8,2)	0.878	2.47	3.59	10.9	0.32		0.069 [45]
(8,5)	0.354	2.41	4.45	22.4	0.058		
(9,0)	4.02	0	3.52	0	0.19	0.08 [11]	0.17 [7]
							0.17 [43]
							0.08 [43]
							0.093 [44]
							0.096 [45]
							0.20 [46]
(9,3)	1.12	0.564	4.32	13.9	0.11		0.02 [47]
(9,6)	0.922	0.827	5.12	23.4	0.035		
(10,1)	0.382	0.594	4.12	4.72	0.20		
(10,4)	0.644	1.33	4.89	16.1	0.13		
(10,7)	0.272	1.85	5.79	24	0.038		
(11,2)	0.332	2.89	4.75	8.21	0.13		
(11,5)	0.284	1.17	5.55	17.8	0.074		
(11,8)	0.243	2.31	6.47	24.8	0.026		
(12,0)	4.02	0	4.70	0	0.042	0.042 [11]	0.040 [44]
							0.078 [45]
							0.08 [45]
(12,3)	0.877	0.449	5.38	10.9	0.076		
(12,6)	1.52	0.374	6.21	19.1	0.078		
(12,9)	0.661	0.594	7.14	25.3	0.013		
(13,1)	0.297	0.464	5.30	3.67	0.14	0.18 [48]	
(13,4)	0.261	1.47	6.03	13.0	0.084		
(13,7)	0.229	0.946	6.89	20.1	0.049		
(13,10)	0.201	1.91	7.82	25.7	0.015		
(14,2)	0.532	0.413	5.91	6.59	0.13		
(14,5)	0.236	1.33	6.68	14.7	0.062		
(14,8)	0.417	0.861	7.55	21.1	0.045		
(14,11)	0.185	2.26	8.50	26.0	0.011		
(15,0)	4.02	0	5.87	0	0.022	0.029 [11]	0.023 [45]
							0.028 [44]
							0.030 [46]
(15,3)	0.722	0.372	6.54	8.95	0.050		
(15,6)	0.644	0.886	7.33	16.1	0.029		
(15,9)	0.574	0.791	8.22	21.8	0.015		
(15,12)	0.515	0.464	9.17	26.3	0.006		
(16,1)	0.243	0.380	6.47	3.00	0.080		
(16,4)	0.877	0.337	7.18	10.9	0.089		

Table 1. (Contd.)

Nanotube	Structural parameters of a nanotube				Band gap width, eV		
	h, au	ω, rad	R, Å	θ, deg	LACW	exp.	ab initio LCAO
(16,7)	0.197	2.73	7.99	17.3	0.058		
(16,10)	0.354	1.21	8.98	22.4	0.025		
(16,13)	0.160	1.95	9.85	26.9	0.011		
(17,2)	0.222	2.97	7.08	5.50	0.065		
(17,5)	0.201	2.57	7.81	12.5	0.057		
(17,8)	0.182	0.751	8.66	18.3	0.022		
(17,11)	0.165	1.12	9.56	22.9	0.015		
(17,14)	0.150	2.23	10.5	26.8	0.009		
(18,0)	4.02	0	7.045	0	0.009		0.02 [44]
(18,3)	0.612	0.317	7.70	7.59	0.038		
(18,6)	1.12	0.282	8.47	13.90	0.030		
(18,9)	1.52	0.249	9.32	19.1	0.034		
(18,12)	0.922	0.413	10.24	23.41	0.018		
(18,15)	3.41	0.380	11.20	27.0	0.003		

increase in radius R and chirality angle θ should lead to a decrease in the band gap width according to the equation [8, 21]:

$$E_g \sim \frac{\cos 3\theta}{R^2}. \qquad (3)$$

The increase in n_2 is accompanied by an increase in R and θ (Table 1).

For the (9,0) tube, $E_g = 0.19$ eV obtained by the LACW method can be compared with the experimental value $E_g = 0.08$ eV measured for the tube on a gold substrate and with the energies predicted by the ab initio LCAO method: 0.08 [43], 0.093 [44], 0.096 [45], 0.17 [7], 0.17 [43] (calculation with correction for electron−electron interaction), and 0.20 eV [46]. For the (9,3) tube, the LACW method gives $E_g = 0.11$ eV; the pseudopotential gap, 0.02 eV, seems to be strongly underestimated [47]. Going from the zigzag (9,0) tube with a ninefold symmetry axis to the low-symmetry (10,1) tube has nearly no effect on the band gap width. The same is valid for the (9,3) and (10,4) tubes and for the (9,6) and (10,7) tubes. The (11,n_2) tubes with $n_2 =$ 2, 5, and 8, the radii and chirality angles are noticeably larger than those of the (9,n_2) tubes; correspondingly, the optical gaps of the (11,n_2) tubes are ~30% smaller. Among the nine (9,n_2), (10,n_2), and (11,n_2) tubes, only three tubes—(9,6), (10,7), and (11,8) with maximal R and θ values—have $E_g < 0.040$ eV; i.e., their optical gaps fall into the THz range. In the series of the (9,n_2), (10,n_2), and (11,n_2) tubes, the gaps decrease roughly linearly with an increase in n_2. As distinct from the simple π-electron model, which implies that the increase in n_2 must always lead to the narrowing of the band gap, the LACW method predicts that a non-

monotonic dependence of E_g on n_2 in the series of the (12,n_2) tubes with $n_2 = 0$, 3, 6, and 9. The largest band gaps $E_g = 0.076$ and 0.077 eV are observed for $n_2 = 3$ and 6; they are almost twice as large as a gap of 0.042 eV for the (12,0) tube. Only the (12,9) tube with the maximal n_2 and $E_g = 0.013$ eV meets the requirements of THz technologies. The band gap energy $E_g = 0.042$ eV obtained by the LACW method for the (12,0) tube coincides exactly with the experimental value for the nanotube deposited onto a gold substrate [11] and can be compared with the previous quantum-chemical data ($E_g = 0.040$, 0.078, and 0.08 eV) [44–46]. According to Eq. (3), transition from the (12,0) tube to the (13,1) and (14,2) tubes should be accompanied by a decrease in E_g, but the LACW method predicts a threefold increase in the gap width to 0.14 and 0.13 eV, respectively. The (13,1) nanotube is the only chiral nanotube for which the experimental band gap width 0.18 eV is known [48]. Table 1 demonstrates that the gap width decreases monotonically with an increase in n_2 in the series (13,n_2) with $n_2 = 1$, 4, 7, 10 and (14,n_2) with $n_2 = 2$, 5, 8, 11. Only for the (13,10) and (14,11) tubes, with maximal n_2 values and, hence, with minimal gaps of 0.015 and 0.011 eV, these band gaps are within the THz range. In going from the achiral (15,0) tube to the chiral (15,3) tube, the band gap width increases from 0.022 to 0.050 eV, while a further increase in n_2 in the (15,n_2) series is accompanied by a decrease in the band gap width to 0.029, 0.015, and 0.006 eV for the (15,6), (15,9), and (15,12) tubes. Only for the (15,0) nanotube, the predicted band gap width $E_g = 0.022$ eV can be compared with the experimentally determined band gap 0.029 eV [11] for the tube on a gold substrate and with the ab initio LCAO values
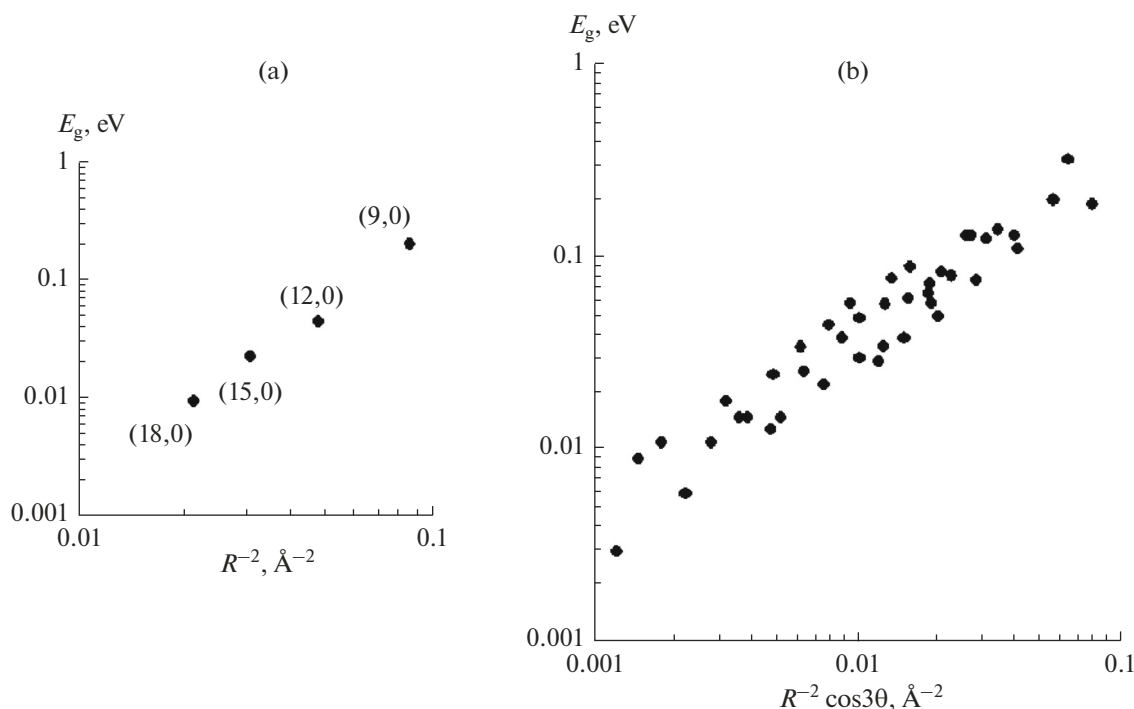
Fig. 2. Dependence of the band gap width on radius and chirality: (a) achiral $(n,0)$ tubes and (b) chiral tubes.

0.023 [45], 0.028 [44], and 0.030 eV [46]. At small n_2 values, the gaps for the $(16,n_2)$ and $(17,n_2)$ nanotubes are larger than those for $(15,n_2)$ analogues; as expected, the increase in n_2 is accompanied by a decrease in the gap width. The gap widths of nearly half of these tubes fall into the THz range. For all the $(18,n_2)$ nanotubes, the E_g values are in the range from 0.003 to 0.038 eV; i.e., all these gaps are in the THz range. As the n_2 index increases, the gap width first increases from $E_g = 0.009$ eV to $E_g = 0.030 - 0.038$ eV and then decreases to 0.003 eV at $n_2 = 15$. Figure 2 shows the dependences of E_g on the radius and chirality of nanotubes.

Thus, the band structure of 50 chiral and achiral (n_1,n_2) tubes with $4 \leq n_1 \leq 18$ and $n_2 = n_1 - 3q$ has been calculated by the LACW method. The nanotubes with optical gaps falling into the terahertz range have been identified, which can be used for creating molecular electronics elements operating in the high-frequency range.

REFERENCES

1. N. Hamada, S. I. Sawada, and A. Oshiyama, Phys. Rev. Lett. **68**, 1579 (1992).

2. R. Saito, M. Fujita, G. Dresselhaus, and M. S. Dresselhaus, Phys. Rev. B **46**, 1804 (1992).

3. R. Saito, M. Fujita, G. Dresselhaus, and M. S. Dresselhaus, Appl. Phys. Lett. **60**, 2204 (1992).

4. C. T. White, D. H. Robertson, and J. W. Mintmire, Phys. Rev. B **47**, 5485 (1993).

5. M. S. Dresselhaus, G. Dresslhaus, and R. Saito, Carbon **3**, 883 (1995).

6. J. W. Mintmire, D. H. Robertson, and C. T. White, J. Phys. Chem. Solids **54**, 1835 (1993).

7. X. Blase, L. X. Benedict, E. L. Shirley, and S. G. Louie, Phys. Rev. Lett. **72**, 1878 (1994).

8. C. L. Kane and E. J. Mele, Phys. Rev. Lett. **78**, 1932 (1997).

9. L. F. Chibotaru, S. A. Bovin, and A. Ceulemans, Phys. Rev. B **66**, 161401(R) (2002).

10. R. R. Hartmann and M. E. Portnoi, IOP Conf. Ser.: Mater. Sci. Eng. **79**, 012014 (2015).

11. M. Ouyang, J. L. Huang, C. L. Cheung, and C. M. Lieber, Science **292** (5517), 702 (2001).

12. M. E. Itkis, S. Niyogi, M. E. Meng, et al., Nano Lett. **2**, 155 (2002).

13. F. Borondocs, K. Kamarás, M. Nikolou, et al., Phys. Rev. B **74**, 045431 (2006).

14. A. Pekker and K. Kamara, Phys. Rev. B **84**, 075475 (2011).

15. T. Kampfrath, K. von Volkmann, C. M. Aguirre, et al., Phys. Rev. B **101**, 267403 (2008).

16. A. W. Bushmaker, V. V. Deshpande, S. Hsieh, et al., Phys. Rev. Lett. **103**, 067401 (2009).

17. H. H. Mantsch and D. Naumann, J. Mol. Struct. **64**, 1 (2010).

18. A. M. Nemilentsau, G. Y. Slepyan, S. A. Maksimenko, et al., *The Handbook of Nanophysics*, vol. 4: *Nanotubes and Nanowires*, Ed. by K. D. Ch. Sattler, 2010, chapter 5, p. 1.

19. R. R. Hartmann and M. E. Portnoi, AIP Conf. Proc. **1705**, 020046 (2016).

20. M. E. Portnoi, O. V. Kibis, and M. R. Costa, Superlattices Microstruct. **43**, 399 (2008).

21. R. R. Hartmann, J. Kono, and M. E. Portnoi, Nanotecnology **25**, 322001 (2014).

22. D. Mann, Y. K. Kato, A. Kinkhabwala, et al., Nat. Nanotechnol. **2**, 33 (2007).

23. T. Mueller, M. Kinoshita, M. Steiner, et al., Nat. Nanotechnol. **5**, 27 (2010).

24. X. Wang, L. Zhang, Y. Lu, et al., Appl. Phys. Lett. **91**, 261102 (2007).

25. S.-W. Chang, J. Hazra, M. Amer, et al., ACS Nano **9**, 11551 (2015).

26. Z. Zhong, N. M. Gabor, J. E. Sharping, et al., Nat. Nanotechnol. **3**, 201 (2008).

27. X. Cui, M. Freitag, R. Martel, et al., Nano Lett. **3**, 783 (2003).

28. S. Choi, Efficient antennas for terahertz and optical frequencies. A Dissertation. Univ. of Michigan (2014).

29. D. F. Santavicca and D. E. Prober, *33rd International Conference on Infrared, Millimeter and Terahertz Waves, IEEE*, Pasadena, CA, 2008.

30. K. Fu, R. Zannoni, S. H. Chan, et al., Appl. Phys. Lett. **92**, 033105 (2008).

31. V. V. Deshpande, B. Chandra, R. Caldwell, et al., Science **323**, 206 (2009).

32. M. R. Amer, A. Bushmaker, and S. B. Cronin, Nano Lett. **12**, 4843 (2012).

33. H. Lin, J. Lagoute, V. Repain, et al., Nat. Mater. **9**, 235 (2010).

34. J. C. Slater, Phys. Rev. **51**, 851 (1937).

35. O. K. Andersen, Phys. Rev. B **12**, 3060 (1975).

36. D. D. Koelling and G. O. Arbman, J. Phys. F: Met. Phys. **5**, 2041 (1975).

37. P. N. D'yachkov, Int. J. Quantum Chem. **116**, 174 (2016).

38. P. N. D'yachkov and D. V. Makaev, Int. J. Quantum Chem. **116**, 316 (2016).

39. P. N. D'yachkov, D. Z. Kutlubaev, and D. V. Makaev, Phys. Rev. B **82**, 035426 (2010).

40. P. N. D'yachkov and D. V. Makaev, Phys. Rev. B **76**, 195411 (2007).

41. P. N. D'yachkov and D. V. Makaev, Phys. Rev. B **74**, 155442 (2006).

42. P. N. D'yachkov, V. A. Zaluev, S. N. Piskunov, and Y. F. Zhukovskii, RSC Adv. **5**, 91751 (2015).

43. T. Miyake and S. Saito, Phys. Rev. B **72**, 073404 (2005).

44. O. Gülseren and T. Yildirim, Phys. Rev. B **65**, 153405 (2002).

45. V. Zólyomi and J. Kürti, Phys. Rev. B **70**, 085403 (2002).

46. G. Sun, J. Kürti, M. Kertesz, et al., J. Phys. Chem. B **107**, 6924 (2003).

47. S. Reich, C. Thomsen, and P. Ordejon, Phys. Rev. B **65**, 155411 (2002).

48. M. R. Amer, S.-W. Chang, R. Dhall, et al., Nano Lett. **13**, 5129 (2013).

Translated by G. Kirakosyan